Laser and Particle Beams (2006), *24*, 157–161. Printed in the USA.

DOI: 10.1017/S0263034606060228

Ion focusing effect of electron cloud produced by laser-plasma interaction

SHUJI MIYAZAKI,[1] NOBUYASU OKAZAKI,[2] RYO SONOBE,[2] QING KONG,[3]
SHIGEO KAWATA,[2]A.A. ANDREEV,[4] AND JIRI LIMPOUCH[5]

[1]Department of Material Science and Engineering, Utsunomiya University, Tochigi, Japan
[2]Department of Electrical and Electronic Engineering, Utsunomiya University, Tochigi, Japan
[3]Institute of Modern Physics, Fudan University, Shanghai, China
[4]Institute for Laser Physics, St Petersburg, Russia
[5]Institute of Physics, Czech Technical University Academy of Sciences of the Czech Republic, Praha, Czech Republic

(RECEIVED 15 June 2005; ACCEPTED 19 September 2005)

Abstract

We propose a focusing mechanism of high-energy ions by an electron cloud produced by a laser interaction with slab plasma. In our 2.5-dimensional (2.5D) particle-in-cell simulations, the laser intensity is 2×10^{20} W/cm^2, the laser wavelength λ is 1.053 μm, and the laser spot size is 2.5λ. When the high intensity laser irradiates slab plasma, electrons are accelerated, oscillate around the plasma and produce the electron cloud locally at the sides of the plasma. Because the electrons are localized transversely, a static electric potential is formed to focus ions and at the same time the ions are accelerated longitudinally. Though the longitudinal ion acceleration has been studied well, the ion focusing effect is reported for the first time in this paper. In our calculations, the maximum energy and intensity of the protons are 8.61 MeV and 1.89×10^{17} W/cm^2, and the diameter of the proton bunch accelerated are focused to 71.2% of its initial size.

Keywords: Electron cloud; Ion acceleration; Ion focusing

1. INTRODUCTION

In recent years, we have seen remarkable progresses in laser intensity improvement (Mourou *et al*., 1998; Strickland & Mourou, 1985), and new particle acceleration schemes have been explored, such as electron acceleration in a vacuum (Hafizi *et al*., 1997; Kawata *et al*., 1991; Kong *et al*., 2003; Malka & Miquel, 1997), high-energy ion production (Allen *et al*., 2003; Nakamura & Kawata, 2003; Passoni & Lontano, 2004; Pommiers & Lefebvre, 2003; Ramirez *et al*., 2004; Shorokhov & Pukhov, 2004; Wilks *et al*., 2001; Chen & Wilks 2005). There was also a remarkable progress in the simulation of high intensity laser plasma interactions, which were discussed recently (Lebo *et al*., 2004; Limpouch *et al*., 2004). When an intense laser irradiates thin slab plasma, electrons are accelerated by the laser and oscillate around the plasma (Kawata *et al*., 2005). Therefore, the electrons accelerated produce an electron cloud at the sides of the plasma (see e.g., Nakamura & Kawata, 2003). The electron cloud extracts and accelerates ions. This acceleration mechanism is well known in laser-plasma interactions.

In this paper, we study an ion focusing mechanism in an interaction of intense laser and thin slab plasma by using 2.5-dimensional (2.5D) particle-in-cell (PIC) simulations. The electron cloud generated on the opposite side of the irradiation surface of laser is formed locally in the transverse and longitudinal directions. Therefore, a static electric potential is formed as well by the electron cloud, and ions are focused and accelerated by the strong static electric potential. Consequently, even in the slab plasma target, one can expect the progress of ion focusing effect. In our ion acceleration and focusing mechanism, a magnetic field influences the electrons and the static electric potential. We also investigated an influence of the magnetic field on our mechanism.

The simulation model and parameters are presented in Section 2. In Section 3, the simulation results of proton focusing and acceleration processes are presented. In Section 4, the conclusions are described.

Address correspondence and reprint requests to: Shuji Miyazaki, Utsunomiya University, Department of Material Science and Engineering, Yohtoh 7-1-2, Utsunomiya 321-8585, Japan. E-mail: dt030106@cc.utsunomiya-u.ac.jp

2. SIMULATION MODEL

Figure 1 shows the schematic view of the calculation model. The slab plasma consists of an Al^{+11} layer of 0.5 μm thickness with an additional 1.5 μm linearly-changing density slope, and an H^+ layer of 0.5 μm thickness. The peak density of Al^{+11} is a solid density and the H^+ plasma is in its solid density. At the initial time, the temperature of plasma ions and electrons are in the Maxwell distribution with 10 KeV and 100 KeV, respectively. The laser intensity is 2×10^{20} W/cm^2, the wave length of laser λ is 1.053 μm, the laser spot size w_0 is 2.5λ, and the duration of Gaussian laser pulse τ is 10 fs. The laser propagates in the x direction and is polarized in the y direction. The center of laser is at $y = 6\lambda$. In this paper, the target side irradiated by the laser is called the laser side and the other side is called the rear side.

3. SIMULATION RESULTS

In this section, the simulation results of proton acceleration and focusing mechanism are presented. In order to clarify a detail of proton focusing and acceleration, we show in Figure 2 the time developments of distributions of high-energy (>2.0 MeV) electrons, static electric potential, and magnetic field. The laser peak reaches the target at t = 27.6 fs. The electrons are accelerated strongly by the laser and generate the electron cloud at the rear side. In this paper, we focus on the rear side for practical reasons. Therefore, a static electric potential is generated, and protons are accelerated by this static electric potential longitudinally, and obtain a MeV order of energy in the parameter range employed in this paper. In our calculations, the spot size of laser is small compared with the target width. Therefore, the electrons accelerated are localized in the rear side and produce the static electric field locally as shown in Figure 2a and Figure 2b. To investigate the detail of localized static electric potential, a precise distribution of static electric potential is shown in Figure 3. The localization of the static electric potential can be seen clearly in Figure 3. The protons are extracted and accelerated from the rear side by this localized static electric potential. Consequently, the proton divergence in the transverse direction is suppressed and protons are focused on the center. A strong magnetic field is

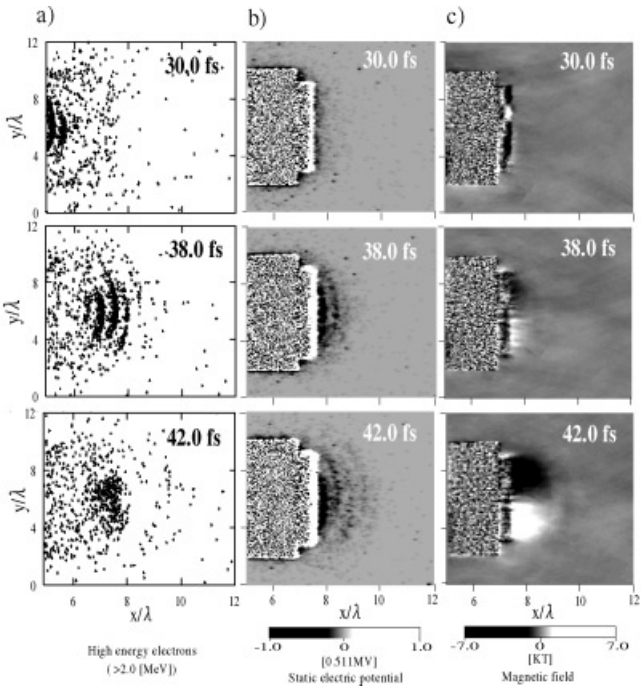

Fig. 2. The time development of distribution of (**a**) the high-energy (>2.0 MeV) electrons, (**b**) the static electric potential, and (**c**) the magnetic field. Each distributions are corresponding to the time of t = 30.0 fs, t = 38.0 fs, and t = 42.0 fs, respectively.

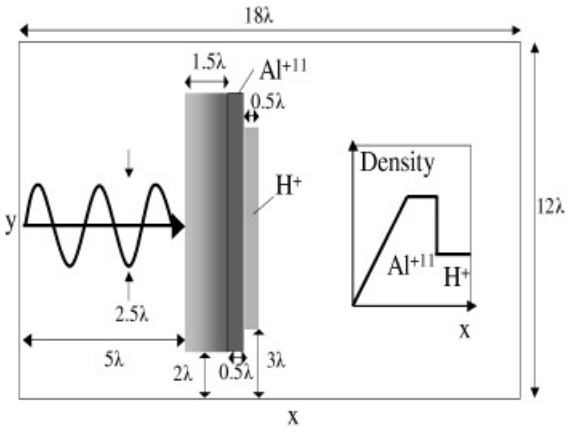

Fig. 1. A schematic view of calculation model. The slab plasma consists of an Al^{+11} layer of 0.5 μm thickness with an additional 1.5 μm linearly-changing density slope and a H^+ layer of 0.5 μm thickness. The laser propagates in the x direction and is polarized in the y direction. The laser center is at $y = 6\lambda$.

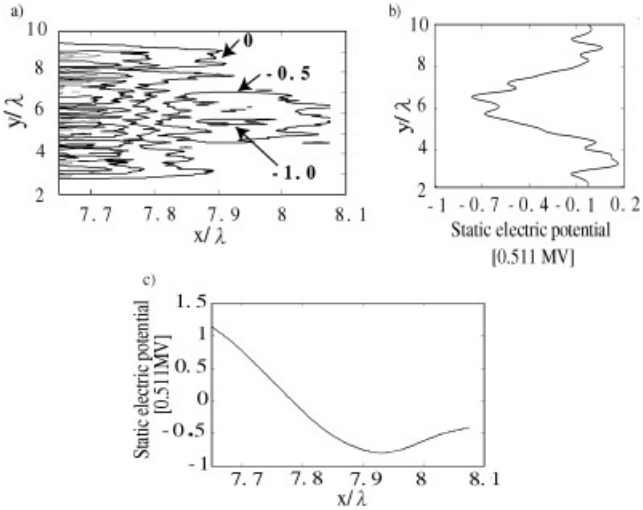

Fig. 3. Distribution of the static electric potential (**a**) in the x-y plane, (**b**) versus y at $x = 7.85\lambda$, and (**c**) versus x at $y = 6.0\lambda$ at t = 42.0 fs.

https://doi.org/10.1017/S0263034606060228 Published online by Cambridge University Press

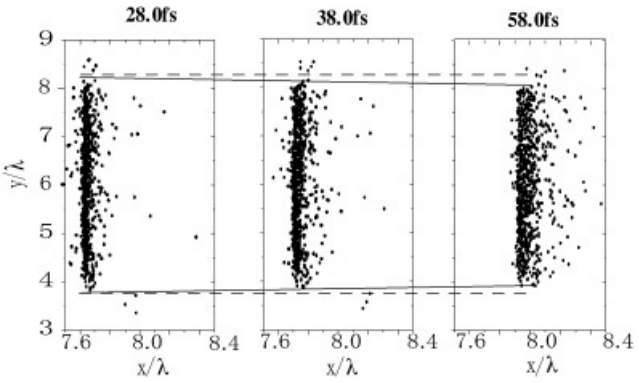

Fig. 4. The maps of proton bunch focused at $t = 28.0$ fs, $t = 38.0$ fs, and $t = 58.0$ fs.

also produced by the electrons accelerated in the rear side as shown in Figure 2c. The magnetic field may influence the electrons motion and consequently may have an influence on the form of static electric potential. The magnetic effect is important in our ion focusing and acceleration mechanism. The analyses of the magnetic field effect are described later on this paper. Figure 4 shows the distributions of the proton bunch focused at $t = 28.0$ fs, $t = 38.0$ fs, and $t = 58.0$ fs, respectively. The divergence of the protons is suppressed by the static electric potential, and the protons are accelerated and slightly focused on the center. In this specific case, the maximum proton energy is 8.61 MeV, and the average proton energy is 0.672 MeV. Figure 5a and Figure 5b shows the time developments of the intensity distributions of the protons bunch accelerated in the transverse and longitudinal directions at $t = 26.0$ fs, $t = 36.0$ fs, and $t = 58.0$ fs. The protons are extracted and accelerated by the localized static electric potential. Consequently, the intensity of proton beam increases near the center. The maximum intensity of proton bunch is 1.89×10^{17} W/cm^2 at $t = 58.0$ fs. A diameter of the proton bunch accelerated at $t = 58.0$ fs is decreased to 71.2% compared with $t = 22.0$ fs. Here the diameter of the proton bunch accelerated is defined by the intensity FWHM of the proton bunch. Figure 2 to Figure 5 show clearly that the protons are focused and accelerated by the localized electron cloud and the generated electric potential. As shown in Figure 2c, one can imagine that the magnetic field can have an influence on the proton focusing. Figure 6 shows results without the influence of the magnetic field: in this case, the magnetic field is set to zero in the equation of motion in order to check the magnetic effect on the proton focusing, though the Maxwell equation is fully solved. Figure 6a, Figure 6b, and Figure 6c show the distributions of high-energy electron (>2.0 MeV), the static electric potential, and the magnetic field at $t = 42.0$ fs in the case without the magnetic field effect. The detail of the static electric potential is presented in Figure 7. Figure 6a show that the electrons are slightly diffused in transverse, and the magnetic field in the rear side is weak as shown in Figure 6c. Consequently, the static electric potential in the rear side is weak and it is also relatively flat as shown in Figure 6b and Figure 7.

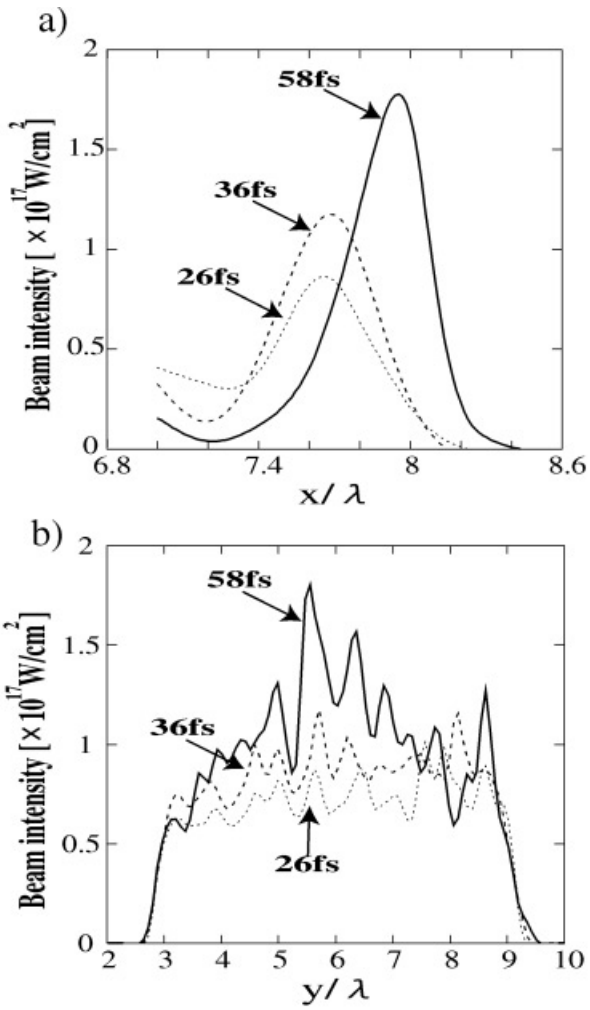

Fig. 5. The intensity distribution of protons bunch accelerated (**a**) versus x and (**b**) versus y at $t = 26.0$ fs, $t = 36.0$ fs, and $t = 42.0$ fs.

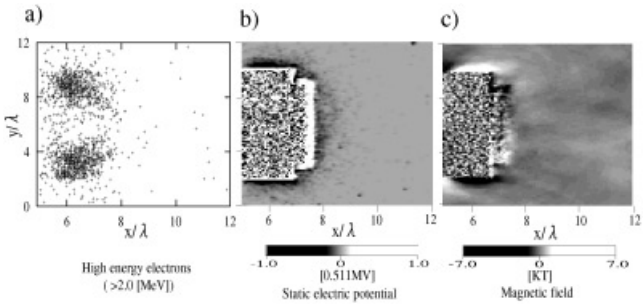

Fig. 6. The distributions of (**a**) the high-energy electrons, (**b**) the static electric potential, and (**c**) the magnetic field at $t = 42.0$ fs. In this calculation, the magnetic field is set to zero in order to investigate the effect of magnetic field on the proton focusing, though the Maxwell equation is fully solved.

https://doi.org/10.1017/S0263034606060228 Published online by Cambridge University Press

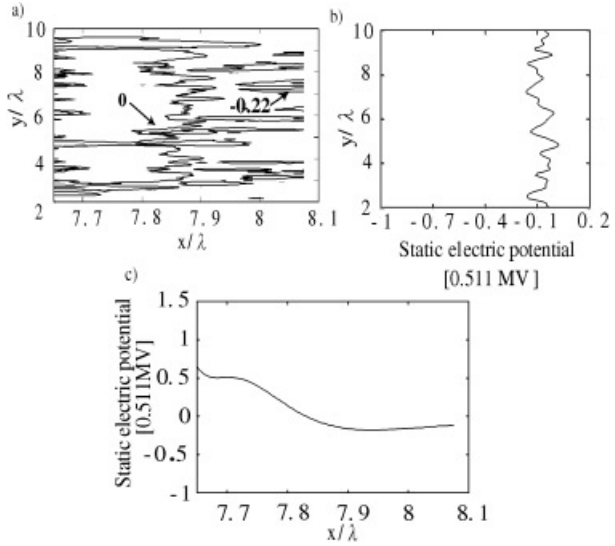

Fig. 7. The details of the static electric potential (**a**) in the *x*-*y* plane, (**b**) versus *y* at $x = 7.85\lambda$, and (**c**) versus *x* at $y = 6.0\lambda$ at $t = 42.0$ fs.

Figure 8 shows the intensity distribution of proton bunch accelerated in the *y* direction. In this specific case, the protons are not well focused by the static electric potential. Therefore, the intensity is nearly flat and the peak of intensity is decreased compared with that in Figure 5. The peak intensity of proton bunch accelerated is 1.24×10^{17} W/cm^2, the maximum proton energy is 8.59 MeV, and the averaged energy is 0.353 MeV. Figure 6, Figure 7, and Figure 8 demonstrate that the magnetic field influences the distribution of the electron cloud and the static potential, and consequently the protons are focused much.

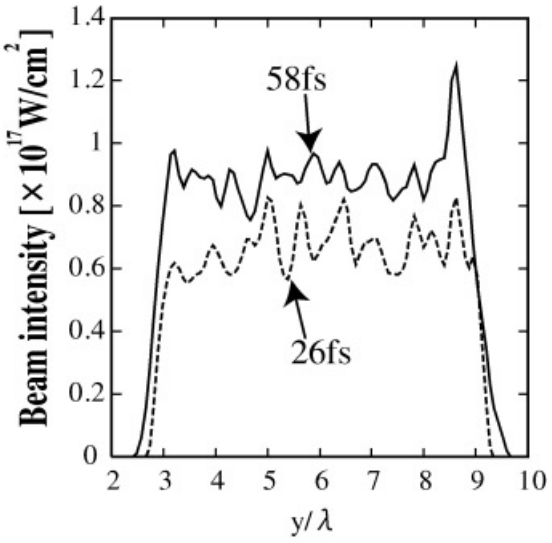

Fig. 8. The intensity distribution of proton bunch accelerated versus *y* direction at $t = 26.0$ fs and $t = 58.0$ fs.

4. CONCLUSIONS

In this paper, the proton bunch focusing and acceleration effects are clarified and demonstrated by the particle simulations. The proton focusing effect comes from the localization of the electron cloud and the static electric potential. In our study, the effect of magnetic field is also investigated. The strong magnetic field has a great influence on the proton focusing effect.

ACKNOWLEDGMENTS

The authors would like to extend their thanks to Prof. K. Mima, Prof. K. Tachibana, Prof. K. Nakajima, Prof. S. Kurokawa, and Prof. N. Yugami for their valuable discussions and suggestions on this subject. This work was performed partly under the collaboration program of the Institute of Laser Engineering, Osaka University and supported in part by the grant in aid for science research under JSPS (Japan Society for the Promotion of Science).

REFERENCES

Allen, M., Sentoku, Y., Audebert, P., Blazevic, A., Cowan, T., Fuchs, J., Gauthier, J.C., Geissel, M., Hegelich, M., Karsch, S., Morese, E., Patel, P.K. & Roth, M. (2003). Proton spectra from ultraintense laser-plasma interaction with thin foils: Experiments, theory, and simulation. *Phys. Plasmas* **10**, 3283–3289.

Chen, H. & Wilks, S.C. (2005). Evidence of enhanced effective hot electron temperatures in ultraintense laser-solid interactions due to reflexing. *Laser Part. Beams* **23**, 411–416

Hafizi, B., Esarey, E. & Sprangle, P. (1997). Laser-driven acceleration with Bessel beams. *Phys. Rev. E* **55**, 3539–3545.

Kawata, S., Maruyama, T., Watanabe, H. & Takahashi, I. (1991). Inverse-bremsstrahlung electron acceleration. *Phys. Rev. Lett.* **66**, 2072–2075.

Kawata, S., Kong, Q., Miyazaki, S., Miyauchi, K., Sonobe, R., Sakai, K., Nakajima, K., Masuda, S., Ho, Y.K., Miyanaga, N., Limpouch, J. & Andreev, A.A. (2005). Electron bunch acceleration and trapping by ponderomotive force of an intense short-pulse laser. *Laser Part. Beams* **23**, 61–67.

Kong, Q., Miyazaki, S., Kawata, S., Miyauchi, K., Nakajima, K., Masuda, S., Miyanaga, N. & Ho, Y.K. (2003). Electron bunch acceleration and trapping by the ponderomotive force of an intense short-pulse laser. *Phys. Plasmas* **10**, 4605–4678.

Lebo, I.G., Demchenko, N.N., Iskakov, A.B., Limpouch, J., Rozanov, V.B. & Tishkin, V.F. (2004). Simulation of high-intensity laser-plasma interactions by use of the 2D Lagrangian code "ATLANT-HE". *Laser Part. Beams* **22**, 267–273.

Limpouch, J., Klimo, O., Bina, V. & Kawata, S. (2004). Numerical studies on the ultrashort pulse K-α emission sources based on femtosecond laser-target interactions. *Laser Part. Beams* **22**, 147–156.

Malka, G. & Miquel, J.L. (1997). experimental observation of electrons accelerated in vacuum to relativistic energies by a high-intensity laser. *Phys. Rev. Lett.* **78**, 3314–3317.

Mourou, G., Barty, C.P.J. & Perry, M.D. (1998). Ultrahigh-intensity lasers: Physics of the extreme on a tabletop. *Phys. Today* **51**, 22–28.

Nakamura, T. & Kawata, S. (2003). Origin of protons acceler-

https://doi.org/10.1017/S0263034606060228 Published online by Cambridge University Press

ated by an intense laser and the dependence of their energy on the plasma density. *Phys. Rev. E* **67**, 026403.

Passoni, M. & Lontano, M. (2004). One-dimensional model of the electrostatic ion acceleration in the ultraintense laser-solid interaction. *Laser Part. Beams* **22**, 163–169.

Pommiers, L. & Lefebvre, E. (2003). Simulation of energetic proton emission in laser-plasma interaction. *Laser Part. Beams* **21**, 573–581.

Ramirez, J., Ramis, R. & Sanz. J. (2004). One-dimensional model for a laser-ablated slab under acceleration. *Laser Part. Beams* **22**, 183–188.

Shorokhov, O. & Pukhov, A. (2004). Ion acceleration in overdense plasma by short laser pulse. *Laser Part. Beams* **22**, 175–181.

Strickland, D. & Mourou, G. (1985). Compression of amplified chirped optical pulses. *Opt. Commun.* **56**, 219–221.

Wilks, S.C., Langdon, T.E., Roth, M., Singh, M., Hatchett, S., Key, M.H., Pennington, D., Mackinnon, A. & Snavely. R.A. (2001). Energetic proton generation in ultra-intense laser-solid interactions. *Phys. Plasmas* **8**, 542–549.

https://doi.org/10.1017/S0263034606060228 Published online by Cambridge University Press